

5. THE POLES—F. Fetterer, Ed.

a. Arctic—J. Richter-Menge, Ed.

1) OVERVIEW—J. Richter-Menge

The permanent presence of sea ice, ice sheets, and continuous permafrost are unique features of the polar regions. The Arctic is further distinguished because it sustains a human population in a harsh environment. These characteristics amplify the impact of global climate change on both the regional physical and societal systems. These impacts reach beyond the Arctic region. For instance, studies are underway to determine the extent to which the loss of sea ice cover and the conversion of tundra to larger shrubs and wetlands, observed to have occurred over the last two decades, have impacted multiyear persistence in the surface temperature fields, especially in the Pacific sector. In this chapter observations collected in 2007, combined with historical records, provide insights into continuing trends in the state of physical components of the Arctic system, including the atmosphere, ocean, sea ice cover, and land.

In 2007 there continued to be widespread evidence of the impact of a general warming trend in the Arctic region, where surface air temperatures reached their highest level on record. One of the most dramatic signals was the significant reduction in the extent of the summer sea ice cover and in the relative amount of older, thicker ice, both showing signs of an increase in the relative rate of reduction. Accompanying the reduction in sea ice cover was an increase in the temperature and a decrease in the salinity of the surface ocean layer. Water temperatures in deeper ocean layers also increased due to the influx of warmer waters into the Arctic Basin. On land, there was a general greening of tundra and browning of forested areas. Permafrost temperatures tended to increase and snow extent tended to decrease. Measurements of the mass balance of glaciers and ice caps indicate that in most of the world, glaciers are shrinking in mass. The largest of these, Greenland, experienced records in both the duration and extent of the summer surface melt.

2) ATMOSPHERE—J. Overland, J. Walsh, and M. Wang

The year 2007 was the warmest on record for the Arctic, continuing a general, Arctic-wide warming trend that began in the mid-1960s (Fig. 5.1). The AO circulation regime, widely considered the main source of Arctic climate variability during the twentieth century, returned to a strongly positive wintertime index value for the first time in more than a decade, but was still lower than the large positive values of the early 1990s (Fig. 5.2). A positive AO is associated

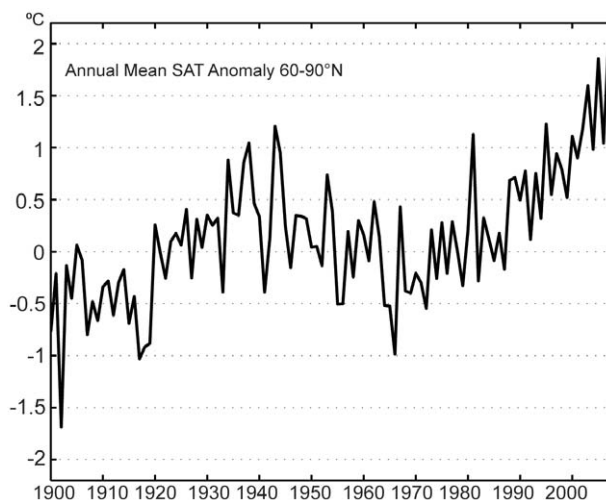


FIG. 5.1. Arctic-wide annual averaged surface air temperature anomalies (60°–90°N) based on land stations north of 60°N relative to the 1961–90 mean. From the CRUTEM3v dataset, (available online at www.cru.uea.ac.uk/cru/data/temperature/).

with lower pressure over Arctic regions and higher pressure at midlatitudes. The SLP anomaly field for winter–spring (December–May) 2007 shows low anomalies over most of the Arctic with a minimum over northern Europe (Fig. 5.3, left). This pattern contrasts with that of the canonical positive AO, where the lowest anomalies are centered over Iceland and the central Arctic. The geostrophic wind pattern associated with the 2007 SLP anomaly field brought air flow from western Russia toward the North Pole, with a positive (warmer) SAT anomaly maximum over the northern Barents Sea (Fig. 5.4, left). During the previous years of weak and variable AO (1996–2006), the geostrophic wind flow anomaly was generally from the Pacific toward the North Pole with positive SAT

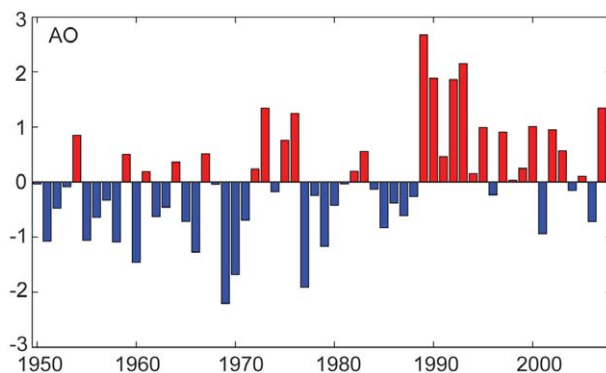


FIG. 5.2. The extended winter (DJFM) Arctic Oscillation index, 1950 to 2007 (based on data available online at www.cpc.ncep.noaa.gov/).

anomalies north of eastern Siberia. It is difficult to say whether the strong positive AO will be sustained. There are historical examples of both single strong AO years and years where the anomaly is the beginning of a multiyear event.

A similarity of 2007 with the early years of the twenty-first century is the nearly Arctic-wide extent of positive SAT anomalies in winter, spring, and fall. These years contrast with the twentieth century in which positive and negative SAT anomalies were more evenly distributed. This Arctic-wide back-

ground SAT anomaly of greater than $+1^{\circ}\text{C}$ is consistent with projections from IPCC climate models (Chapman and Walsh 2007a). The exceptions are the Bering Sea and western Alaska, which were experiencing a third consecutive cold or average winter as 2007 came to a close.

The Arctic-wide negative SLP anomaly pattern of winter and spring was followed in summer by an unusually strong high pressure region in the Beaufort Sea and low SLP over central Russia (Fig. 5.3, right) that set up sustained geostrophic winds blowing from

the North Pacific across the North Pole. These winds contributed to sea ice advection toward the Atlantic sector and the advection of warm moist air into the central Arctic, and to a record minimum Arctic sea ice cover in September (see section 5a4). The summers of 2005 through 2007 all ended with extensive areas of open water. As a result, freeze-up occurred later than usual, and surface air temperature remained high into the following autumn, with warm SAT anomalies above $+6^{\circ}\text{C}$ during October and November across the central Arctic. Such autumn SAT anomalies are also consistent with sea ice extent projections from IPCC climate model simulations performed with increasing greenhouse gas concentrations.

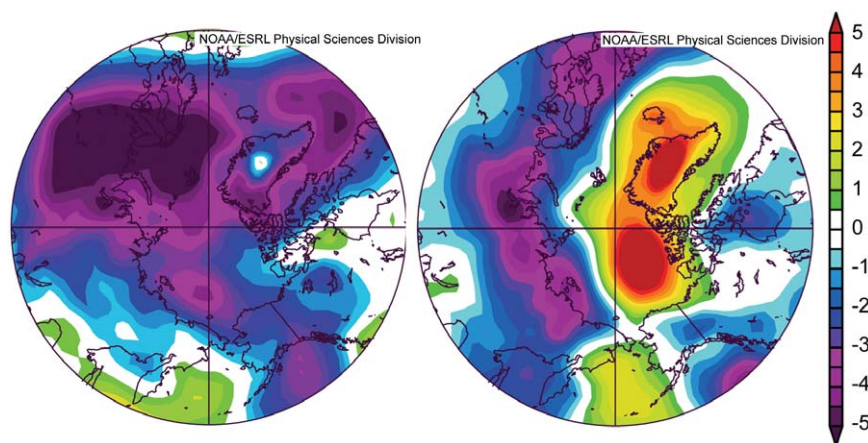


FIG. 5.3. SLP anomaly pattern for (left) Dec 2006–May 2007 and (right) Jun–Aug 2007. Note the extensive Arctic-wide areas of low SLP in winter and spring, which project onto a positive AO index. Data are from the NCEP–NCAR reanalysis through the NOAA/Earth Systems Research Laboratory, generated online at www.cdc.noaa.gov. Anomalies are relative to a 1968–96 climatological period.

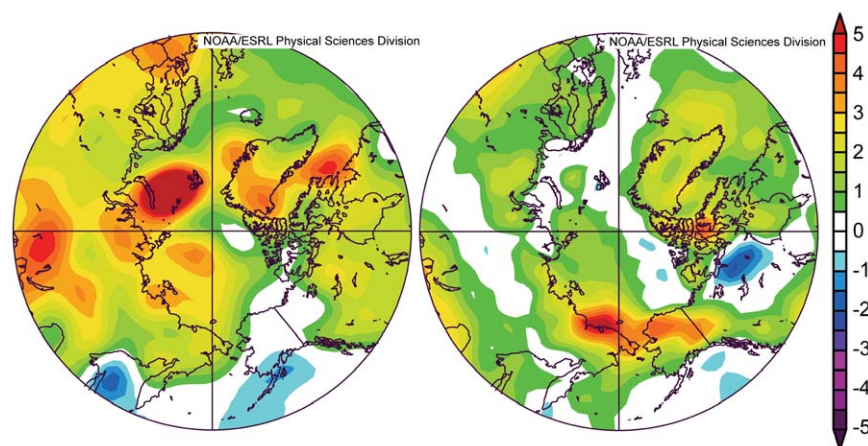


FIG. 5.4. Similar to Fig. 5.3, but for surface air temperature anomalies in $^{\circ}\text{C}$ for (left) Dec 2006–May 2007 and (right) Jun–Aug 2007. Note the nearly Arctic-wide positive values in winter and spring. In summer, melting ice keeps air temperature near the surface close to zero. After fall freeze-up, air temperature anomalies exceeded 6°C over much of the Arctic Ocean (not shown). Anomalies are relative to a 1968–96 climatological period.

- 3) OCEAN—A. Proshutinsky, J. Morison, I. Ashik, E. Carmack, I. Frolov, J. C. Gascard, M. Itoh, R. Krishfield, F. McLaughlin, I. Polyakov, B. Rudels, U. Schauer, K. Shimada, V. Sokolov, M. Steele, M.-L. Timmermans, and J. Toole

(i) Circulation

In 2007, the ocean surface circulation regime in the Beaufort Sea was strongly anticyclonic (clockwise) in winter and summer (Fig. 5.5).

In winter the major flow stream removed sea ice from the Kara and Laptev Seas, while in the summer sea ice from the Canada Basin was transported out quickly by strong winds. Data from satellites and drifting buoys indicate that the entire period of 1997–2007 was characterized by an anticyclonic ocean surface circulation regime in the Beaufort region. This circulation pattern was the result of a higher sea level atmospheric pressure over the Beaufort Gyre, relative to the 1948–2007 mean, and the prevalence of anticyclonic winds.

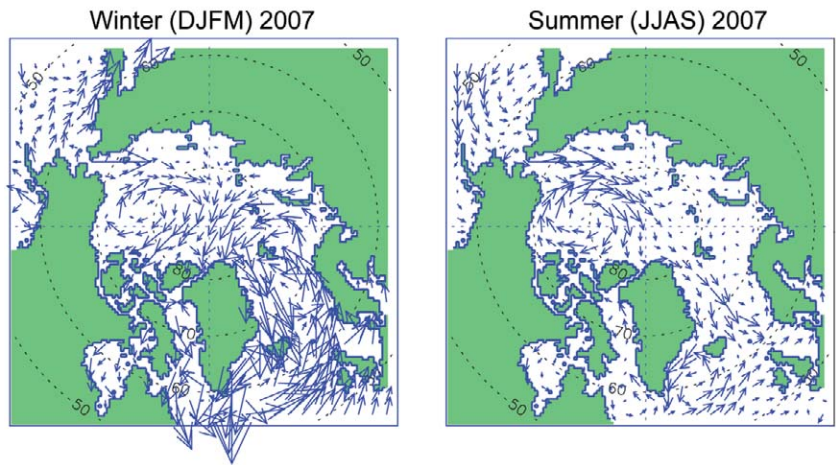


FIG. 5.5. Circulation patterns of the simulated upper-ocean wind-driven circulation in (left) winter and (right) summer of 2007. Updated following Proshutinsky and Johnson (1997).

(ii) *Water temperature and salinity*

(A) *MARGINAL SEAS*

SST trends over the past 100 yr in the Arctic marginal seas (White, Kara, Laptev, East Siberian, Chukchi, and Beaufort) were analyzed by Steele et al. (2008). They found that many areas cooled up to $\sim 0.5^\circ\text{C decade}^{-1}$ during 1930–65 as the AO index generally fell (see Fig. 5.2), while these areas warmed during 1965–95 as the AO index generally rose. Warming is particularly pronounced since 1995, and especially since 2000 when the AO index exhibited relatively low and fluctuating values. Summer 2007 satellite-derived data indicate that SST anomalies were up to 5°C in ice-free regions (Fig. 5.6).

Long-term (1930–95) salinity trends (Steele and Ermold 2004) show that since 1930, the White Sea has gained freshwater while the East Siberian Sea has lost it, consistent with river discharge trends over this period. Over the past 20 yr, increases in both river discharge and direct precipitation can explain ob-

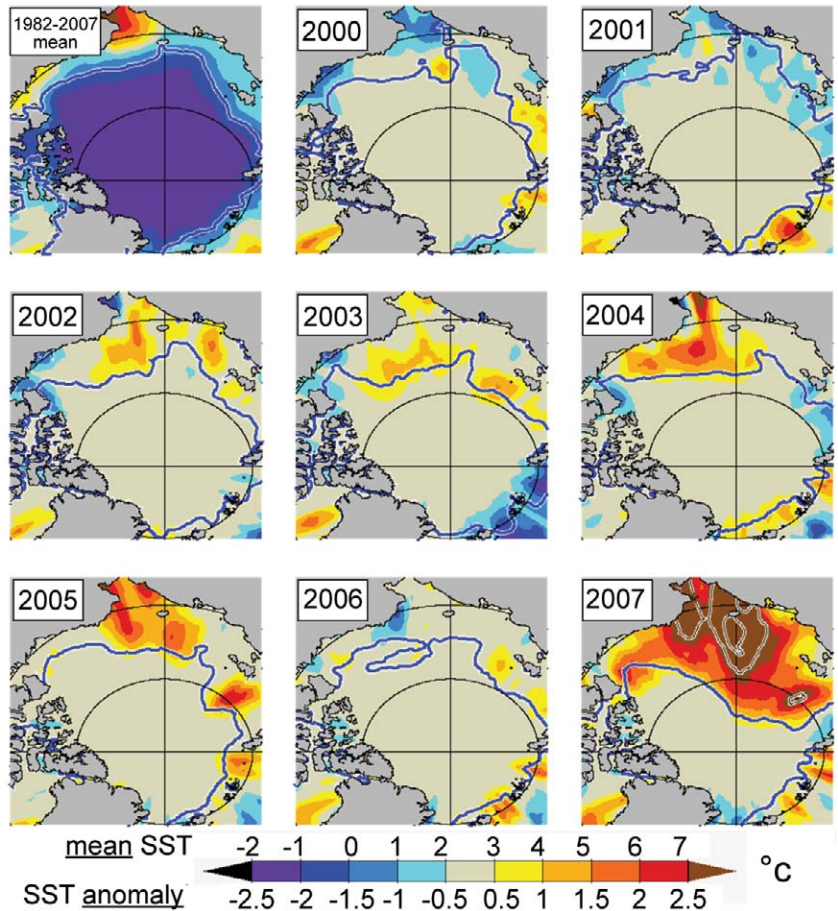


FIG. 5.6. (top left) Mean satellite-derived summer (Jul–Aug) SST (Reynolds et al. 2002) and anomalies from this mean over 2000–07. Latitudes 70° and 80°N and longitudes $0^\circ/180^\circ$ and $90^\circ\text{E}/270^\circ\text{E}$ are shown. For 2007, extra contours for 3° and 4°C are provided. Also shown is the Sep mean ice edge (blue contour) for each year (from Steele et al. 2008).

served salinity decreases in the White Sea, but not in the Kara Sea. Salinity trends in the Laptev Sea and East Siberian Sea indicate that ocean circulation plays a dominant role in these areas, where in recent years freshwater has been diverted eastward along the coast, rather than northward toward the deep ocean. Polyakov et al. (2008) confirmed these results and extended the data analysis up to 2003. The result shows that the freshwater content trend in the Siberian Seas (upper 50-m layer) for the period 1920–2003 is $29 \pm 50 \text{ km}^3 \text{ decade}^{-1}$. In 2007, all expeditions working in the marginal seas (I. Polyakov et al. 2007, personal communication) indicated an unusual freshening of the surface layer due to an extreme rate of sea ice melt.

(b) *CENTRAL ARCTIC (NANSEN, AMUNDSEN, AND MAKAROV BASINS)*

In spring 2007 near surface salinities at the NP were increased by about 1 unit and the AW core temperature was increased by 0.5°C , respectively, above pre-1990s climatology. Data collected since 2000 at the NPEO (<http://psc.apl.washington.edu/northpole/>) indicate that in 2000 and 2001 the spring salinities in the upper 150 m near the pole and in the northern Makarov Basin were elevated 1–2 units above climatology and temperatures in the Atlantic Water core along the Lomonosov Ridge were elevated $1^\circ\text{--}2^\circ\text{C}$. These conditions were nearly the same as observed in 1993 (Morison et al. 2000). In spring of 2004 and 2005, NP region hydrographic conditions largely returned to climatology (Morison et al. 2006). In spring of 2006, temperature and salinity anomalies near the NP region began to move away from climatological norms, again, repeating their behavior in spring of early 2000–03. The 2007 International Polar Year expansion of NPEO airborne surveys, combined with observations of the Switchyard project (W. Smethie 2007, personal communication), yielded a springtime section across $90^\circ\text{W}\text{--}90^\circ\text{E}$. Results from this survey were consistent with the NP data, a further indication that in 2007 upper-ocean salinity structure and Atlantic Water temperatures in the central Arctic Ocean moved away from climatological norms, with increased salinity and temperature.

Atlantic Water enters the Arctic Ocean through the Barents Sea and Fram Strait, where it transitions from surface water to water of intermediate depth. The Atlantic Water temperature increase can be partially explained by other observed changes in the AW layer circulation. The first evidence of strong warming within the AW layer was found in the Nansen Basin in 1990 (Quadfasel et al. 1991).

Positive AW anomalies of up to 1°C were carried along the continental margins into the Arctic Ocean interior (Woodgate et al. 2001; Schauer et al. 2002). Schauer et al. (2004) and Polyakov et al. (2005) have also shown that since the late 1990s, AW temperature has increased. Polyakov et al. (2007) and Dmitrenko et al. (2008) found that the 2000–05 Atlantic Water warming along the Siberian continental slope has propagated as a series of several AW warm impulses that penetrated into the Arctic Ocean through Fram Strait in 1999–2000 with a mean speed of 2.5 cm s^{-1} . The 2007 results suggest one of these pulses has reached the central Arctic Ocean. Preliminary reports from the summer hydrographic surveys in the central Arctic (U. Schauer et al. 2007, personal communication) indicate that, relative to 2004–05, in the Nansen and Amundsen Basins the temperature of the Atlantic Water core increased by approximately 0.5°C , and the thickness of this layer increased by 100–150 m mostly due to the propagation of a warming signal into the deeper ocean layers. In the Makarov Basin, no changes in the parameters of the Atlantic Water layer were detected. In contrast to the NPEO springtime results, in all basins the summer surface salinity was 1–2 units less than in 2003–05. It is speculated that the decrease in salinity in these regions is related to the extent of the massive sea ice melt in 2007 (see section 5a4).

(c) *CANADA BASIN AND BEAUFORT GYRE*

The 2007 Canada Basin and the Beaufort Gyre summer conditions exhibited very strong freshening relative to 2006 and previous years of observations (Richter-Menge et al. 2006). Data collected as part of the BGOS (www.whoi.edu/beaufortgyre/index.html) show that in 2000–07, the total freshwater content in the Beaufort Gyre has not changed dramatically relative to climatology (although the absolute maximum was observed in 2007), but there was a significant change in the freshwater distribution (Fig. 5.7c,d). The center of the freshwater maximum shifted toward Canada and significantly intensified relative to climatology. This region of the Beaufort Gyre is much fresher than 30 yr ago.

Significant changes were observed in the heat content of the Beaufort Gyre (Fig. 5.7a,b). It has increased relative to the climatology, primarily because of an approximately twofold increase of the Atlantic layer water temperature (Shimada et al. 2004). In the late 1990s, Atlantic Water with temperatures as much as 0.5°C warmer than previous records was observed in the eastern Canada Basin (McLaughlin et al. 2004). These observations signaled that warm-anomaly

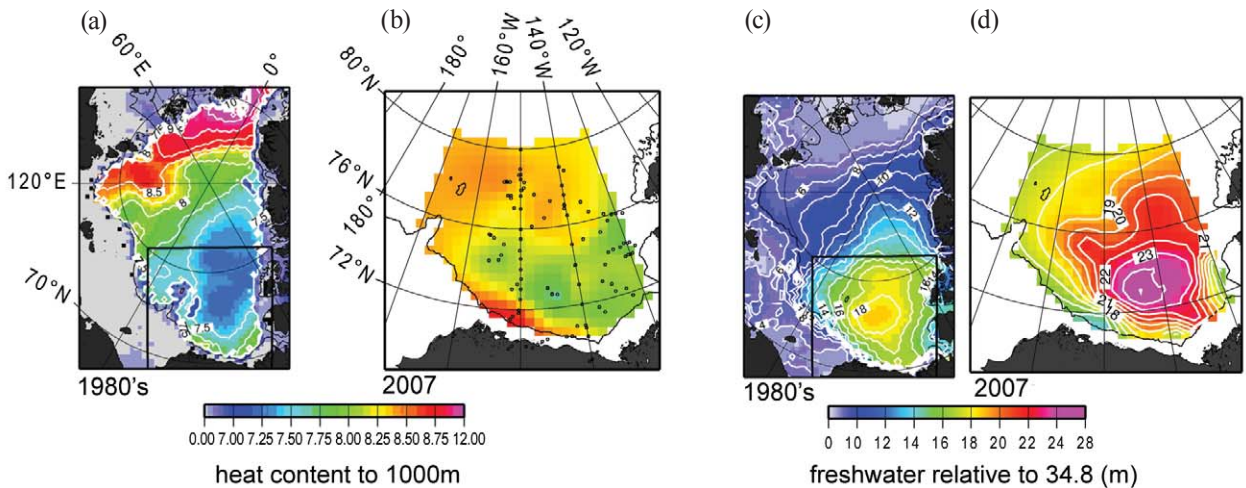


FIG. 5.7. (left) Summer heat ($1 \times 10^{10} \text{ J m}^{-2}$) and (right) freshwater (m) content. (a),(c) Heat and freshwater content in the Arctic Ocean based on 1980s climatology (Timokhov and Tanis 1997). (b),(d) Heat and freshwater content in the Beaufort Gyre in 2007 based on hydrographic survey (black dots depict locations of hydrographic stations). For reference, this region is outlined in black in panels a and c. The heat content is calculated relatively to water temperature freezing point in the upper 1,000-m ocean layer. The freshwater content is calculated relative to a reference salinity of 34.8.

Fram Strait waters, first observed upstream in the Nansen Basin in 1990, had arrived in the Canada Basin, and confirm the cyclonic circulation scheme. The 2007 observations manifested that these processes are still in progress and the AW layer warming signal propagated farther east.

The surface layer water in the Beaufort Gyre also accumulated a significant amount of heat in 2007, due to the significant retreat of the ice cover causing its exposure to the direct solar heating. This was similar to the conditions observed in the regions free of ice in the Amundsen, Nansen, and Makarov Basins.

(iii) Sea Level

Figure 5.8 contains SL time series from nine coastal stations having representative records for the period of 1954–2007 in the Siberian Seas (from the Arctic and Antarctic Research Institute data archives). There is a positive SL trend along Arctic coastlines, which, for 1954–89, after correction for GIA, was $1.94 \pm 0.47 \text{ mm yr}^{-1}$. This compares to an estimated rate of $1.85 \pm 0.43 \text{ mm yr}^{-1}$ along the Arctic coastlines over the same period, based on 40 Arctic coastal stations available at the time (Proshutinsky et al. 2004). The addition of 1990–2007 data increases the estimated rate of SL rise for the nine stations in the Siberian Seas, beginning in 1954, to $2.61 \pm 0.45 \text{ mm yr}^{-1}$ (after correction for GIA).

From the beginning of the record until 1996, SL correlates relatively well with the time series of the

AO index and SLP at the North Pole (Fig. 5.8). In contrast, from 1997–2007 SL generally increased despite the relatively stable behavior of AO and SLP, indirectly indicating that after 1996 something other than the inverted barometric effect dominated sea level rise in the region. Among possible candidates are ocean expansion due to heating, freshening, and wind-driven effects.

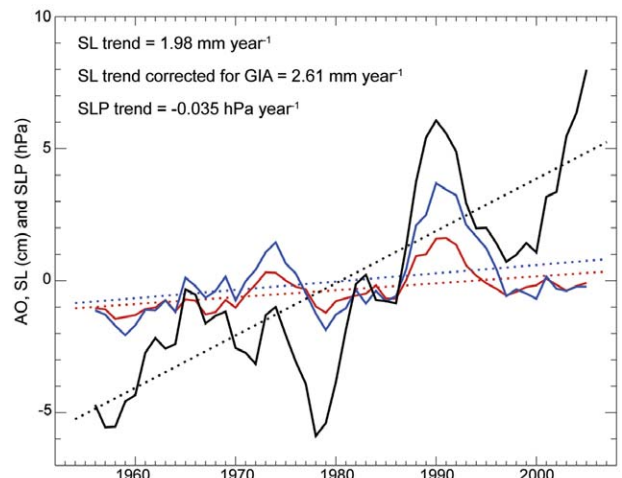


FIG. 5.8. Five-year running mean time series: annual mean sea level at nine tide gauge stations located along the Kara, Laptev, East Siberian, and Chukchi Sea coastlines (black line). The red line is annual mean AO index anomaly multiplied by 3. The blue line is the SLP at the North Pole (from NCAR–NCEP reanalysis data) multiplied by -1 .

4) SEA ICE COVER—J. Richter-Menge, J. Comiso, W. Meier, S. Nghiem, and D. Perovich

(i) *Extent and thickness*

Satellite-based passive microwave images of sea ice cover have provided a reliable tool for continuously monitoring changes in the extent of Arctic ice cover since 1979. During 2007, the summer minimum ice extent, observed in September, reached 4.3 million km² (Fig. 5.9, right panel). This marked a new record minimum, with a dramatic reduction in area of coverage relative to the previous record of 5.6 million km², set just two years ago in 2005. At the end of the 2007 melt season, the sea ice cover was 23% smaller than it was in 2005 and 39% below the long-term average from 1979 to 2000. An extended time series of sea ice extent, derived primarily from operational sea ice charts produced by national ice centers, suggests that the 2007 September ice extent was 50% lower than conditions in the 1950s to the 1970s (Stroeve et al. 2008). The 2007 summer retreat of the ice cover was particularly pronounced in the East Siberian and Laptev Seas, the Beaufort Sea, and the Canadian Archipelago.

The annual maximum sea ice extent occurs each March. In March 2007, the maximum ice extent was 14.7 million km² (Fig. 5.9, left panel). This marked

a slight recovery from the record minimum of 14.4 million km² for the period 1979–2007, which was observed in 2006. Consistent with 2006, the March 2007 ice extent fell within the mean contour at almost every location.

For comparison, the mean monthly ice extent for March and September, for the period 1979–2007, is 15.6 and 6.7 million km², respectively.

The annual variation of the extent of the Arctic sea ice cover in 2007, relative to past years, is shown in Fig. 5.10. As explained in Comiso et al. (2008), the 2007 Arctic ice cover was comparable to the 2005 and 2006 ice covers through mid-June but then began a more precipitous decline. Five-year averages from 1980 through 2004 show a general decrease in the Northern Hemisphere sea ice extent throughout the seasonal cycle, with this pattern being especially strong in the late summer and early fall. The 2007 ice extent rebounded with a rapid early autumn growth, albeit with an exceptionally slow recovery in the Chukchi and Barents Seas. By early November 2007, the ice extent conditions were comparable to those observed in recent years, while remaining well below the long-term (1979–2007) average.

Figure 5.11 shows the time series of the anomaly in ice extent in March and September for the period 1979–2007. Both winter and summer have a negative trend in extent: -2.8% decade⁻¹ for March and -11.3% decade⁻¹ for September. The seasonality of the observed ice retreat is consistent with model projections.

Ice thickness is intrinsically more difficult to monitor. With satellite-based techniques (Laxon et al. 2003; Kwok et al. 2004) only recently introduced, observations have been spatially and temporally limited. Data from submarine-based observations indicate that the ice cover at the end of the melt season thinned by an average of 1.3 m during the period 1956–78 and from 3.1 to 1.8 m in the 1990s (Rothrock et al. 1999). New measurements from ICESat and estimates of thickness using ice age as a proxy indicate the ice has thinned significantly over the last decade (Stroeve et al. 2008; Maslanik et al. 2007).

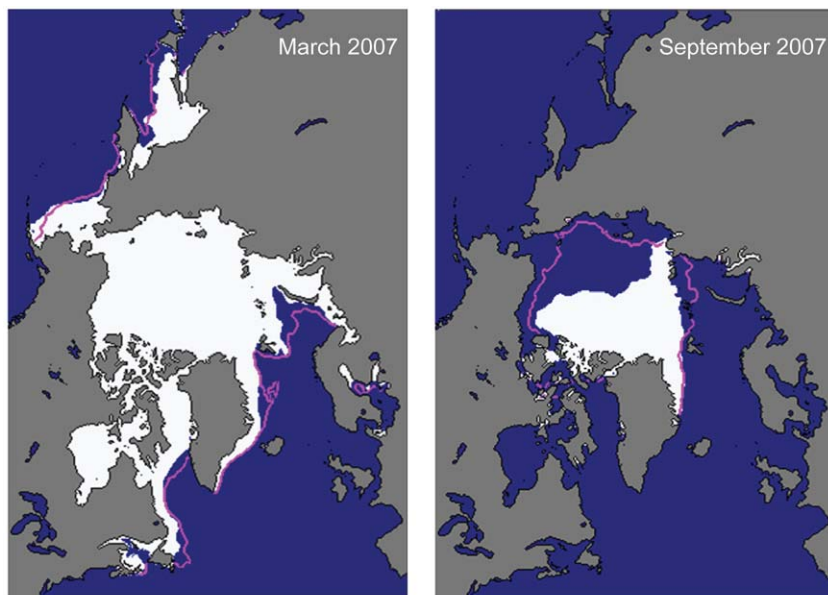


FIG. 5.9. Sea ice extent in (left) Mar and (right) Sep 2007, when the ice cover was at or near its maximum and minimum extent, respectively. The magenta line indicates the median maximum and minimum extent of the ice cover, for the period 1979–2000. The Sep 2007 minimum extent marked a record minimum for the period 1979–2007. [Figures from the National Snow and Ice Data Center Sea Ice Index: nsidc.org/data/seaice_index.]

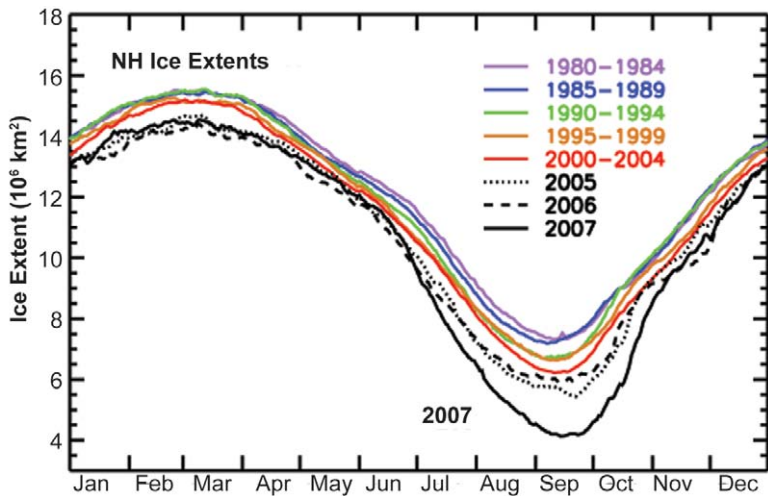


FIG. 5.10. Daily ice extents 2005, 2006, and 2007, and averaged over the 5-yr periods 1980–84 through 2000–04. Values are derived from satellite passive microwave data from NASA’s SMMR and the Department of Defense’s SSM/I. (Adapted from Comiso et al. 2008.)

Measurements of the seasonal and coastal ice cover do not indicate any statistically significant change in thickness in recent decades (Melling et al. 2005; Haas 2004; Polyakov et al. 2003).

(ii) *Seasonal versus perennial ice*

The Arctic sea ice cover is composed of perennial ice (the ice that survives year-round) and seasonal ice (the ice that melts during the summer). Consistent with the diminishing trends in the extent and thickness of the cover is a significant loss of the older, thicker perennial ice in the Arctic (Fig. 5.12). Data

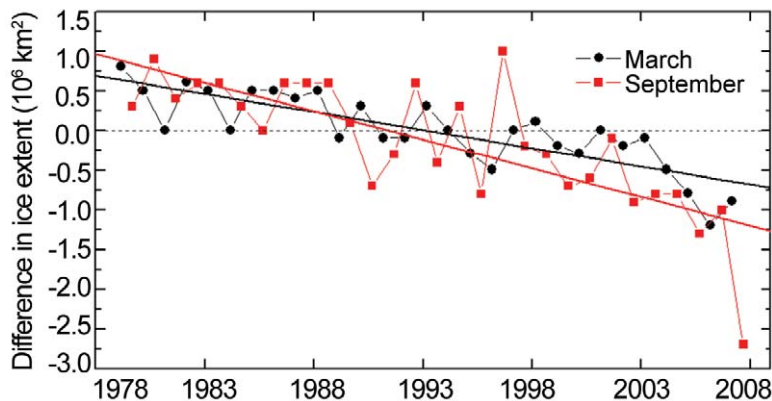


FIG. 5.11. Time series of the difference in ice extent in Mar (the month of ice extent maximum) and Sep (the month of ice extent minimum) from the mean values for the time period 1979–2007. Based on a least squares linear regression, the rate of decrease for the Mar and Sep ice extents was -2.8% and -11.3% per decade, respectively.

from the NASA QSCAT launched in 1999 and the buoy-based DM developed in earlier work by Rigor and Wallace (2004) and Nghiem et al. (2007) indicate that the amount of perennial ice in the March ice cover has decreased from approximately 5.5 to 3.0 million km^2 over the period 1958–2007. While there is considerable interannual variability, an overall downward trend in the amount of perennial ice began in the early 1970s. This trend appears to coincide with a general increase in the Arctic-wide, annually averaged surface air temperature, which also begins around 1970 (see Fig. 5.1). In recent years, the rate of reduction in the amount of older, thicker perennial ice has been increasing, and now very little ice older than 5 yr remains (Maslanik et al. 2007).

The QSCAT and DM techniques are consistent in their indication that the older, thicker ice is concentrated in the western Arctic Basin. This result reflects the recent prevailing ice circulation patterns in the Arctic (see Fig. 5.5). Ice residence times are typically longer in the western Arctic in the region of the Beaufort Gyre. The eastern Arctic is dominated by the Transpolar Drift, which carries sea ice out of the Arctic Basin via the Fram Strait.

Many authors have recently acknowledged that a relatively younger, thinner ice cover is more susceptible to the effects of atmospheric and oceanic forcing (e.g., Gascard et al. 2008; Stroeve et al. 2008; Kwok 2007; Ogi and Wallace 2007; Maslanik et al. 2007; Serreze et al. 2007; Shimada et al. 2006). Warming temperatures (Christensen et al. 2007), atmospheric and oceanic circulation patterns that advect ice out of the Arctic, and the amplification of these effects through the ice albedo feedback mechanism (Perovich et al. 2007) are combining to reduce the area covered by perennial ice.

5) LAND—V. ROMANOVSKY, R. ARMSTRONG, A. SHIKLOMANOV, D. WALKER, AND G. JIA

(i) *Vegetation*

Evidence of widespread changes in vegetation in northern latitudes comes from trends in terrestrial greenness

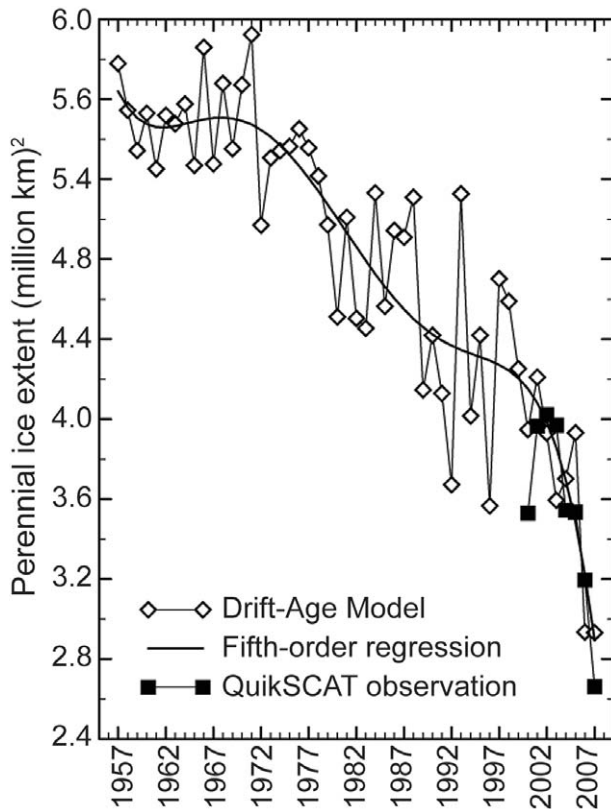


FIG. 5.12. Time series of area of perennial sea ice extent in Mar of each year estimated by the Drift-Age Model (with a fifth-order regression) and observed by QuikSCAT satellite scatterometer within the model domain. In each year, the model result was an average over Mar, and the satellite observation was on the spring equinox (21 Mar). (Adapted from Nghiem et al. 2007.)

as detected by the NDVI derived from the NOAA AVHRR satellites (Myneni et al. 1997; Zhou et al. 2001; Lucht et al. 2002; Jia et al. 2003; Goetz et al. 2005; Bunn et al. 2007). During the 1981–2005 period of observation, about 6% of the circumpolar tundra area experienced an increase in NDVI and about 1% experienced a decrease (Fig. 5.13; Bunn et al. 2007). The positive trends in NDVI in tundra areas have been strongest in North America. For example, in the tundra region south of 70°N (the region of the Arctic with a consistent AVHRR record from 1982 to 2005) the rate of change in NDVI is +0.58% yr⁻¹ over the North American Arctic compared to +0.34% yr⁻¹ over the Eurasian Arctic (Jia et al. 2007). Forested areas experienced a slight decline over the same period: NDVI declined in 6% of the forested area versus an increase in 4% of the area.

Vegetation responds relatively quickly to warming temperatures by growing more vigorously and

densely. Over a longer time span, changing climate alters vegetation type. Land cover on much of the Alaska North Slope, for example, is transitioning from tundra to shrubs (Wang and Overland 2004). Changes in land cover, vegetation density, and other factors are reflected in NDVI. Overall, increasing NDVI is consistent with warming soil and air temperatures, earlier snow melt, and the expansion of shrubs and tree line to the north.

(ii) *Permafrost*

Observations show a general increase in permafrost temperatures during the last several decades in Alaska (Osterkamp and Romanovsky 1999; Romanovsky et al. 2002; Osterkamp 2003; Romanovsky et al. 2007a), northwest Canada (Couture et al. 2003; Smith et al. 2005), Siberia (Pavlov 1994; Oberman and Mazhitova 2001; Romanovsky et al. 2007b; Pavlov and Moskalenko 2002), and northern Europe (Isaksen et al. 2000; Harris and Haeblerli 2003).

Permafrost temperature records uninterrupted for more than 25 yr have been obtained by the University of Alaska Fairbanks along the International Geosphere-Biosphere Programme Alaskan transect, which spans the entire continuous permafrost zone in the Alaskan Arctic. All of the observatories show a substantial warming during the last 20 yr (Fig. 5.14). The detailed characteristic of the warming varies

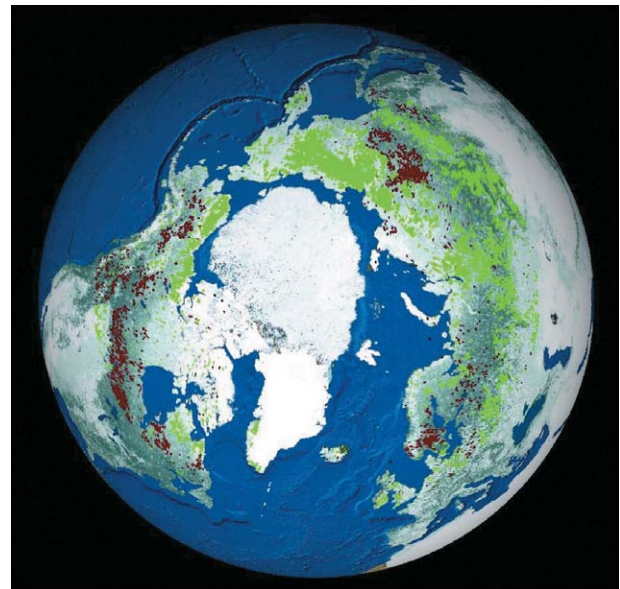


FIG. 5.13. Spatial distribution of trends in May to Aug photosynthetic activity across the northern high latitudes from 1981 through 2005. Significant positive trends in photosynthetic activity are shown in green, and negative trends are shown in rust. (From Bunn et al. 2007.)

between locations, but is typically from 0.5° to 2°C at the depth of zero seasonal temperature variations in permafrost (Osterkamp 2005). These data also indicate that the increase in permafrost temperatures is not monotonic. During the observational period, relative cooling has occurred in the mid-1980s, in the early 1990s, and then again in the early 2000s. As a result, permafrost temperatures at 20-m depth experienced stabilization and even a slight cooling during these periods. Permafrost temperature was relatively stable on the North Slope of Alaska during 2000–06. However, 2007 data show a noticeable increase in the temperature at 20-m depth by 0.2°C at the two northernmost sites of Deadhorse and West Dock. Permafrost temperature did not change significantly at the other North Slope sites. This may indicate a new wave of permafrost warming similar to the warming that started in 1994 (Fig. 5.14), which also started at the Deadhorse and West Dock sites and only later appeared at the interior sites.

(iii) *Snow extent*

Northern Hemisphere snow cover extent has a mean maximum of approximately 47 million km², typically occurring in February. The minimum usually occurs in August and is less than about 1 million km², most of which is snow on glaciers and perennial snow fields. As a result, snow cover is the land surface characteristic responsible for the largest annual and interannual differences in land surface albedo. Snow covers a much smaller area in the Southern Hemisphere, approximately 2% of the global total, and plays a relatively small role in global climate.

Time series of snow extent in the Northern Hemisphere, beginning in 1978 and derived from two sources, consistently show a decreasing trend in snow cover in the months of April through October, with the strongest seasonal signal occurring between April and August (Fig. 5.15). Data derived from NOAA snow charts (Robinson and Frei 2000; Frei and Robinson 1999; Ramsay 1998; NOAA/NESDIS/OSDPD/SSD 2006) indicate a statistically significant decreasing trend of -2.1% decade⁻¹ (Brodzik et al. 2006). Snow cover data derived from passive microwave imagery (Armstrong and Brodzik 2001; Armstrong et al. 2005a,b) show a decreasing trend of -0.7% decade⁻¹, although it is not significant at the 90% level. Both time series show similar inter-annual variability and consistently indicate Northern Hemisphere maximum extents exceeding 40 million km². The western United States is among the regions with the strongest decreasing trends, supporting Groisman et al. (2004) and Mote et al. (2005) results using in

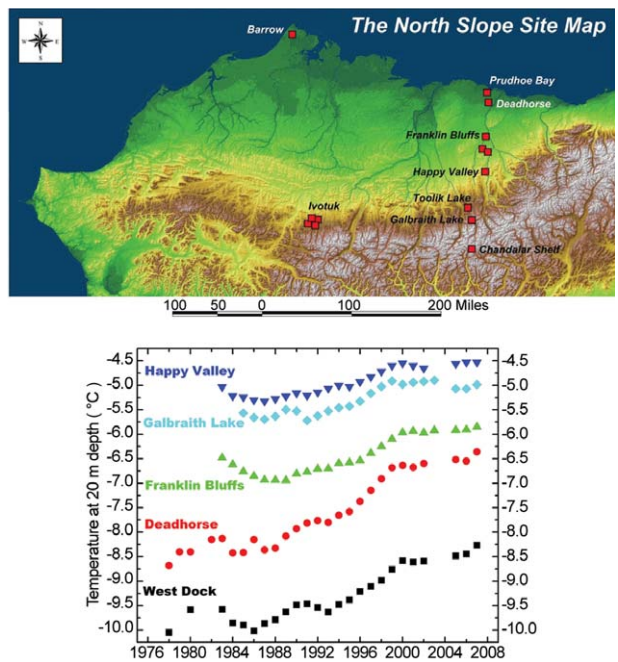


FIG. 5.14. (top) Location of the long-term University of Alaska permafrost observatories in northern Alaska. West Dock is at Prudhoe Bay. (bottom) Changes in permafrost temperatures at 20-m depth during the last 25 to 30 yr (updated from Osterkamp 2003).

situ observations. Shallow snow cover at low elevations in temperate regions is the most sensitive to temperature fluctuations and hence most likely to decline with increasing temperatures (Lemke et al. 2007, 343–346).

For the Northern Hemisphere winter of 2006–07, the microwave data indicate negative departures from the long-term mean (1978–2007) for every month except October and February, with an average negative departure for the winter months (November through April) of approximately 0.7 million km². For the calendar year of 2007, the NOAA data indicate an average snow cover extent of 24.0 million km², which is 1.5 million km² less than the 38-yr average and represents the third least extensive snow extent for the period of record (see section 2c2 for additional information on 2007 Northern Hemisphere snow extent).

(iv) *Glaciers*

Glaciers and ice caps, excluding those adjacent to the large ice sheets of Greenland and Antarctica, can be found on all continents except Australia and have an estimated total area between 512 and 540 × 10³ km². The complicated and uncertain processes that control how fast glaciers move make it difficult

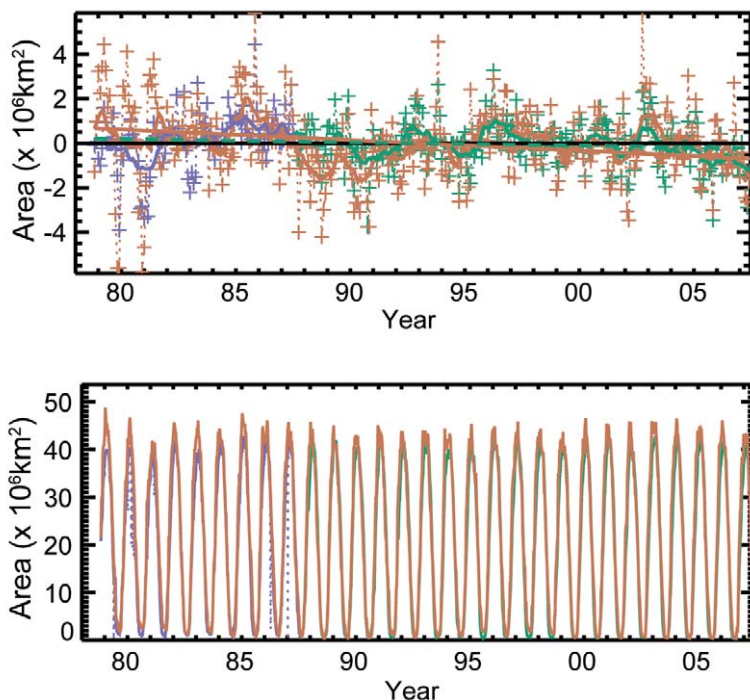


FIG. 5.15. (top) Time series of Northern Hemisphere SCA derived from passive microwave (purple/green) and NOAA snow charts (orange), and (bottom) SCA departures from monthly means, 1978–2007.

to use changes in the areal extent of glaciers as a straightforward indicator of changes in climatic conditions. Mass balance measurements, or the difference between the accumulation and ablation, are a more direct method to determine the year-to-year “health” of a glacier. Changes in mass balance correspond to changes in glacier volume. These measurements are typically obtained from less than about 0.2% of the world’s glaciers. Researchers have measured mass balance on more than 300 glaciers since 1946, with a continuous record for about 40 glaciers since the early 1960s (e.g. Cogley 2005; Kaser et al. 2006).

These results indicate that in most regions of the world, glaciers are shrinking in mass. From 1961 to 2005, the thickness of “small” glaciers decreased approximately 12 m, or the equivalent of more than 9,000 km³ of ice (Dyurgerov and Meier 2005; online at http://nsidc.org/sotc/glacier_balance.html). Recent mass loss of glaciers, ice caps, and ice sheets is estimated to be 0.58 mm SLE per year between 1961 and 2005 and 0.98 mm SLE per year between 1993 and 2005 (Dyurgerov and Meier 2005; online at http://nsidc.org/sotc/sea_level.html). In contrast to the two major ice sheets, Greenland and Antarctica, the network of small glaciers and ice caps, although making up only about 4% of the total land

ice area or about 760,000 km³, may have provided as much as 60% of the total glacier contribution to sea level change since the 1990s. This acceleration of glacier melt may cause 0.1 to 0.25 m of additional sea level rise by 2100 (Meier et al. 2007). The greatest mass losses per unit area are found in Patagonia, Alaska, and northwest United States/southwest Canada. However, because of the corresponding large areas, the biggest contributions in total to sea level rise come from Alaska, the Arctic, and the Asian high mountains.

(v) River discharge

Overall, the twenty-first century to date is characterized by an increased level of river discharge to the Arctic Ocean (www.R-ArcticNet.sr.unh.edu). The mean 2000–06 discharge from six of the largest Eurasian rivers (North Dvina, Pechora, Ob, Yenisei, Lena, and Kolyma) was 127 km³ (7%) higher than long-term mean over the period 1936–99 (Fig. 5.16). The largest Siberian rivers, Yenisey and Lena, provided more than 70% of this increase. Preliminary 2007 estimates of annual discharge to the Arctic Ocean from the Russian rivers have been made using near-real-time data (<http://RIMS.unh.edu>). These estimates indicate a relatively high annual discharge for the six largest Eurasian rivers, possibly achieving a new historical maximum in 2007 for total discharge to the Arctic Ocean over the 1936–2007 observational period.

The mean annual discharge to the ocean over 2000–06 from the five largest North American rivers was about 6% (30 km³) greater than the long-term mean over 1973–99. The historical annual maximum was observed for the summary discharge in 2005 (Fig. 5.16). However, the relatively short discharge time series for North America (37 yr) and the significant unmonitored land area does not support conclusions with the same reliability as for Eurasia.

6) GREENLAND—J. Box, J. Cappelen, D. Bromwich, L.-S. Bai, T. Mote, B. Veenhuis, N. Mikkelsen, and A. Weidick

(i) Synopsis

Greenland experienced regional warming in 2007, with statistically significant positive (warm) annual temperature anomalies in the 1.3° to 2.7°C range for coastal stations and 1.3°C for the inland ice sheet

with respect to the 1971–2000 averages. Seasonal temperature anomalies were largest in winter but not positive in every season. Upper air temperatures indicate lower- to midtropospheric warm anomalies in all seasons above sounding stations surrounding Greenland. Noteworthy are western and southern locations where midtropospheric anomalies exceed those observed at the surface. Ice sheet surface melt duration anomalies were up to 53 days longer than the 1973–2000 average, based on passive microwave remote sensing. MODIS-derived surface albedo anomalies in 2007 versus the 2000–07 period were persistently negative, consistent with extensive surface melting. Greenland’s largest glacier continued its recession, with ice flushing out from an embayment thought to have been ice filled since at least the onset of the Little Ice Age. The overall ice sheet mass budget was likely in mass deficit by at least $100 \text{ km}^3 \text{ yr}^{-1}$.

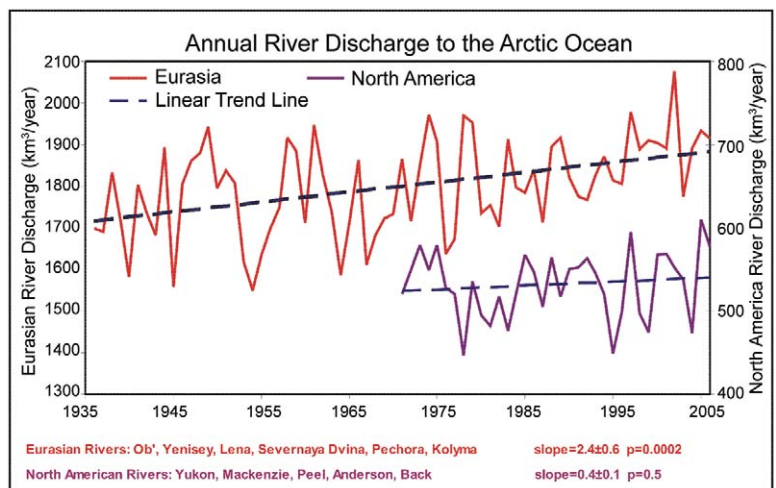


FIG. 5.16. Total annual discharge to the Arctic Ocean from the six largest rivers in the Eurasian pan-Arctic for the observational period 1936–2006 (updated from Peterson et al. 2002) (red line) and from the five largest North American pan-Arctic rivers over 1973–2006 (purple line). The least squares linear trend lines are shown as dashed blue.

(ii) Coastal surface air temperatures

Warm (positive) anomalies predominated in 2007, relative to the last 50-yr period (1958–2007), when con-

TABLE 5.1. Greenland station surface air temperature anomalies by season, 2007 vs 1971–2000. Anomalies are in K. Bold values indicate values that meet or exceed 1 Z-score.

| Station (Region), latitude N, longitude W, time range | Winter | Spring | Summer | Autumn | Annual |
|---|-------------|--------|-------------|------------|------------|
| Pituffik/Thule AFB (NW), 76.5°N, 68.8°W, 1961–2007 | -2.9 | 1.4 | 1.2 | 0.4 | 0.1 |
| Upernavik (NW), 72.8°N, 56.2°W, 1958–2007 | 5.3 | 9.0 | -1.8 | 2.8 | 1.9 |
| Ilulissat (W), 69.2°N, 51.1°W, 1958–2007 | 5.4 | 1.6 | 1.4 | 0.0 | 2.1 |
| Aasiaat (W), 68.7°N, 52.8°W, 1958–2007 | 5.5 | 2.9 | 1.9 | 0.3 | 2.7 |
| Nuuk (SW), 64.2°N, 51.8°W, 1958–2007 | 1.4 | 2.8 | -3.1 | -0.4 | -0.1 |
| Prins Christian Sund (S), 60.0°N, 43.2°W, 1958–2007 | 1.5 | 0.4 | 1.8 | 1.2 | 1.3 |
| Tasiilaq (SE), 65.6°N, 22°W, 1958–2007 | 2.0 | 1.6 | 1.6 | 1.2 | 1.6 |
| Danmarkshavn (NE), 76.8°N, 18.8°W, 1958–2007 | 1.0 | 0.5 | 0.4 | 1.7 | 0.9 |

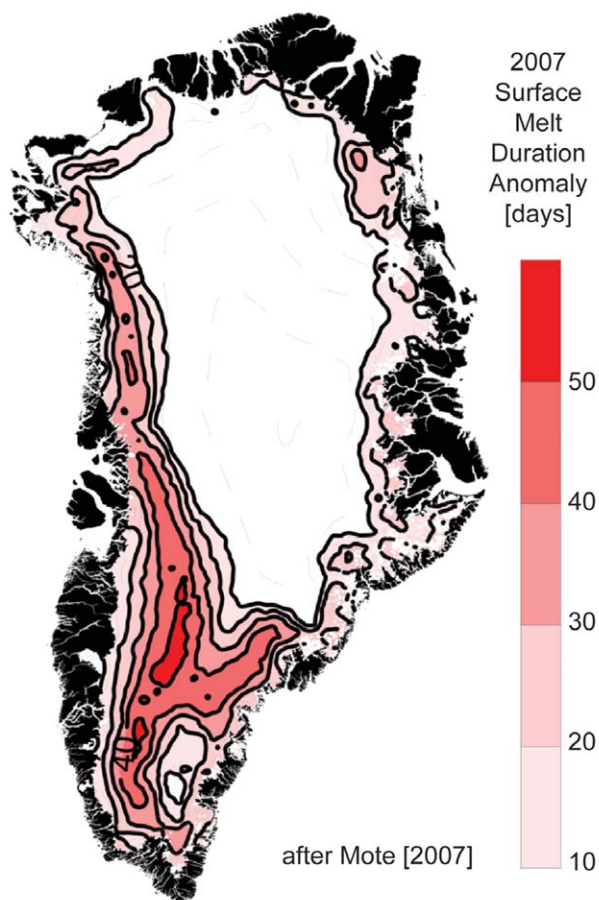


FIG. 5.17. Surface melt duration departure from average for summer (Jun–Aug) 2007 from SSM/I; units are days. The average is based on the summers from 1973 to 2000 (excluding 1975, 1977, and 1978). Only departures >10 days are included. (Figure after Box et al. 2006 and Mote 2007.)

tinuous surface air temperature records are available from a collection of stations around the island (Cappelen et al. 2007, 2008). Exceptions included an anomalously cold winter at Pittufik (northwest), an unusually cold summer and autumn at Nuuk (southwest), and an anomalously cold summer at Upernavik. The Z-scores exceeding ± 1.0 or ± 2.0 indicate anomalies exceeding the most common 66% or 95% of the observed cases, respectively (Table 5.1). At Upernavik (northwest) the spring temperature was the warmest in the past 50 yr, and at Nuuk (southwest) the summer temperature was the coldest in the past 50 yr. The only anomalies that were significant annually, that is, with Z-scores ≥ 1.0 , were warm anomalies for 2007 annual means.

(iii) Upper air temperatures

Upper air sounding data available from the Integrated Global Radiosonde Archive (Durre et al.

2006) indicate for Greenland in 2007 a continued pattern of lower- to midtropospheric warming and lower-stratospheric cooling, consistent with trends since 1964 (Box and Cohen 2006). In the lower troposphere at the 850-hPa level (1.1–1.5-km altitude), for example, annual temperature anomalies were between $+0.6^\circ$ and $+1.5^\circ\text{C}$ at sites surrounding the island, relative to the 1971–2000 average. Seasonal anomalies were largest in winter with $+8.1^\circ\text{C}$ at 1,000 hPa at the Aasiaat/Egedesminde sounding site, with smaller positive anomalies elsewhere in almost all seasons. At the upper limit of mandatory observational levels, (20 hPa, in the lower-mid stratosphere), -11.6°C anomalies are evident. Large lower-stratospheric temperature anomalies are not necessarily abnormal given the relatively large observed temperature variability due in part to much lower atmospheric mass (e.g., Christy and Drouilhet 1994). Summer anomalies above southern Greenland balloon launching sites at the 850 and 600-hPa levels were between 0.2° and 1.3°C .

(iv) Greenland ice sheet melt extent

Passive microwave observations indicate summer 2007 (June–August) SMD was greater than any other observed summer since records began in 1973 (Mote 2007). The ice sheet area undergoing surface melt was 60% greater in 2007 than the next highest year (1998). Summer 2007 had 20 days more melt than average (1973–2000) across nearly all of the regions that exhibit melting. Up to 53 more days of melting than average was observed for elevations in the 2,000- to 2,400-m above sea level range between the north and south domes of the ice sheet (Fig. 5.17).

(v) Ice sheet precipitation, evaporation, and meltwater runoff

Polar MM5 climate data assimilation model runs spanning 50 yr (1958–2007), calibrated by independent in situ ice core observations (Bales et al. 2001; Mosley-Thompson et al. 2001; Hanna et al. 2006) and ablation stakes (van de Wal et al. 2006), indicate that year 2007 precipitation and accumulation was not abnormal despite a $+10 \text{ km}^3 \text{ decade}^{-1}$ positive total precipitation trend over the 1958–2007 period. Surface water vapor fluxes were within an insignificant inter-annual range. In accordance with a $+1.3^\circ\text{C}$ year 2007 annual mean temperature anomaly, the fraction of precipitation that fell as rain instead of snow, surface meltwater production, and meltwater runoff were well above the 1971–2000 mean (Table 5.2). Due to abnormally large mass loss by meltwater runoff despite normal snow accumulation,

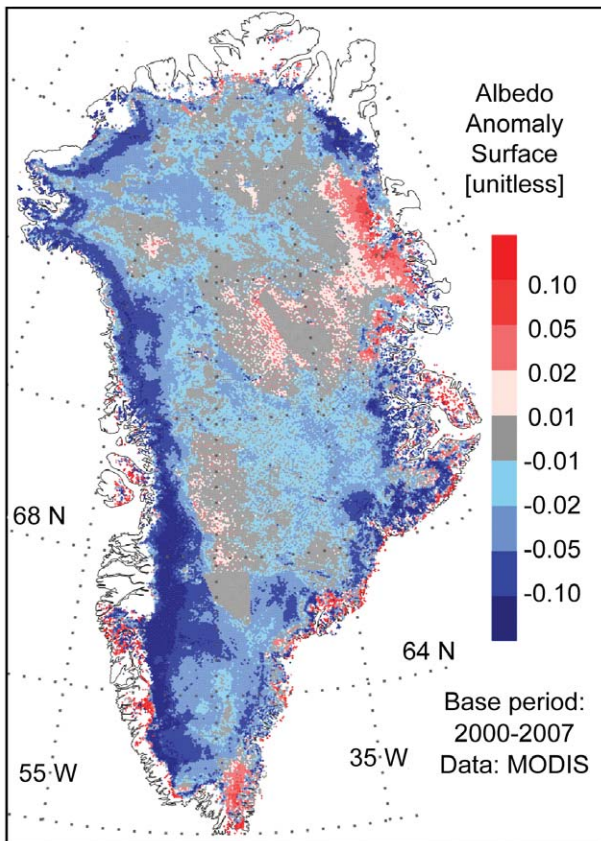


FIG. 5.18. Albedo anomaly (unitless) for 8–23 Aug (days 220–235) 2007 vs the 2000–07 average (from algorithm based on Liang et al. 2005).

the net surface mass budget was 46% below normal, corresponding with a $-156 \text{ km}^3 \text{ yr}^{-1}$ anomaly. The 2007 surface mass budget anomaly was a significant fraction of the accumulation rate of $613 \text{ km}^3 \text{ yr}^{-1}$ for the 1971–2000 period.

(vi) Ice sheet albedo

Surface solar radiation reflectance, referred to as albedo, decreases in response to surface melting. Melt season surface albedo anomalies were calculated using the Liang et al. (2005) algorithm for the 2000–2007 period in 15-day intervals that provided sufficient cloud-free viewing of the surface. Negative surface albedo anomalies were widespread beginning in early June, when melting normally begins, through late August when abnormal

melt and more frequent rainfall darkened the snow and ice surface (Fig. 5.18).

(vii) Glacier changes

The terminus of Greenland’s largest glacier, the Jakobshavn’s Isbrae near Ilulissat, moved 0 to 500 m in 2007 (Fig. 5.19), continuing a retreat that began in 2001 with a dramatic 11-km floating ice collapse (Weidick and Bennike 2007). The large ice lagoon called Tissarissog at the south side of the fjord was flushed of ice by the end of the summer, ice-free probably for the first time since at least the onset of the Little Ice Age (ca. 0.4–0.1 ky BP). It is possible that Tissarissog was ice-free before that time during the medieval warm period (ca. 1.1–0.5 ky BP).

b. Antarctic

1) OVERVIEW—I. A. SCAMBOS

The Antarctic climate system is distinctly different from the Arctic, governed more strongly by the high degree of symmetry of both land and ocean surrounding the pole. The continent’s high plateau anchors a strong polar vortex of westerly winds, and is the source of a near-constant katabatic airflow from a frequent inversion layer near the ice sheet surface. Along its coastline, a narrow zone of easterly flow occurs south of the girdling westerlies. (Captain James Cook noted in 1796 that if he were to try to approach the continent again, he might take advantage of this high-latitude shift in the prevailing winds.) Variations in this westerly flow, and in the relative air pressure between the vortex interior and the encircling regions is the primary oscillation of the far southern climate system, the so-called SAM (Marshall 2003). Another recognized pattern is zonal wave 3 (Raphael



FIG. 5.19. Front position of the Ilulissat (Jakobshavn Isbrae) glacier in 2007 and earlier years, based on Weidick and Bennike (2007). The image mosaic is from Jun 2003 Landsat and ASTER images.

TABLE 5.2. Greenland ice sheet surface mass balance parameters: 2007 departures from 1971–2000 average (adapted from Box et al. 2006).

| Total | 2007 as % of average | 2007 minus average (km ³ yr ⁻¹) |
|--------------------------|----------------------|--|
| Total precipitation | 97% | -18.9 |
| Liquid precipitation | 140% | 8.3 |
| Evaporation | 97% | -2.1 |
| Blowing snow sublimation | 106% | 2.1 |
| Snow accumulation | 97% | -18.9 |
| Meltwater production | 153% | 154.9 |
| Meltwater runoff | 177% | 137.3 |
| Surface mass balance | 64% | -156.4 |
| Mean temperature | — | 1.3 |
| Accumulation area ratio | 93% | -0.064 (%) |

and Holland 2006; Raphael 2004), describing the tendency for a trio of fixed high pressure cells, and adjacent low pressure cells, to dominate circulation patterns about the continent.

increased westerly wind flow. This pattern is consistent with both GHG forcing of climate (Arblaster and Meehl 2006), and with seasonal ozone reduction in the stratosphere (Thompson and Solomon 2002). This

increased tendency toward stronger westerlies tends to isolate the cold continental plateau more, leading to cooling, and drives northwesterly flow over the peninsula, resulting in warming. But, importantly, the stronger westerly flow may be influencing ocean currents as well, moving coastal surface water northeastward via Ekman flow, and as a result drawing a return flow of warmer Antarctic Circumpolar Deep Water onto the continental shelf at depth, thus accelerating basal melt rates of thicker ice masses (e.g., Pine Island glacier; Rignot 2008).

The year 2007 was somewhat anomalous relative to

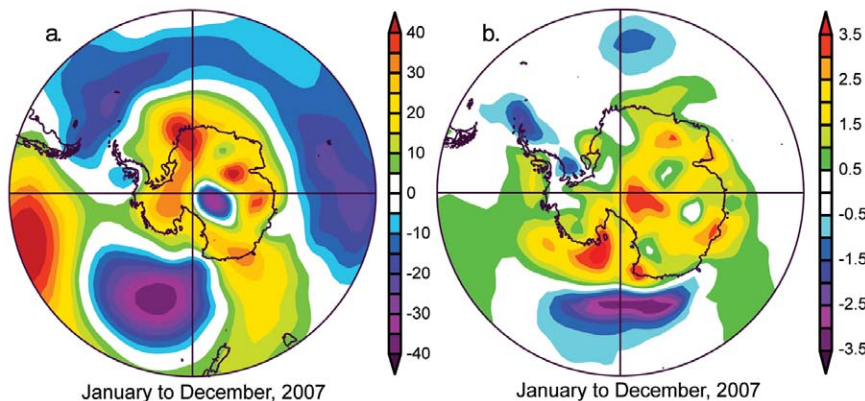


FIG. 5.20. Annual anomaly of (a) 850-hPa geopotential height and (b) surface temperature for 2007 relative to the 1979–2006 period, from NCEP–NCAR reanalysis data. The 850-hPa value is inferred for high-altitude regions of the continent; however, this level best illustrates the near-surface and middle troposphere patterns. These graphs, and climate diagrams shown in Fig. 5.22 (section 5b2), are from the NOAA/ESRL Physical Sciences Division (generated online at www.cdc.noaa.gov). Note that station data for a station near 85°S, 120°E is suspect, particularly for geopotential height, in all NCEP data here.

recent preceding years, with an extended period of negative SAM index, but a sharp rise to strongly positive SAM in December (that persisted into January 2008). The end of the year was likely influenced by the moderate La Niña pattern in the Pacific ENSO circulation. The continent as a whole was warmer than average for the year (underscoring the influence of SAM and the temperature trends in the main continent), and the Antarctic Peninsula was considerably cooler than the period of record (1979 to 2006; see Fig. 5.20b). This resulted in extensive fast ice accumulation on the eastern peninsula coast by the end of the calendar year, and an unusually late start to the summer melt season there. The high degree of variability in the climate pattern led to highly variable sea ice extent anomalies, with monthly mean record highs and record lows being set again this year, as in 2006. Springtime ozone levels were above the record lows of last year, and near the average of the past 15 yr, due to a warmer springtime stratosphere.

2) ATMOSPHERIC CIRCULATION—R. L. Fogt, T. A. Scambos, and S. Barreira

Antarctic circulation anomalies (here, area-averaged 60°–90°S) were near normal for the first half of the year. During austral fall, however, a weaker than normal SAM pattern (Figs. 5.21 and 5.22) allowed for multiple penetrations of warmer maritime air, and generated significant (beyond +2 standard deviations) mid- to lower-tropospheric warming in late fall/early winter (Marshall 2007) while the stratosphere was anomalously cool (< -2 standard deviations). The surface warming in winter, in conjunction with increased planetary wave activity, propagated anomalous heat flux throughout the depth of the troposphere into the stratosphere, leading to marked (>2 standard deviations) geopotential height increases (Fig. 5.21a), reduction of the previously cold stratosphere (Fig. 5.21b), and weakening of the circumpolar vortex (Fig. 5.21c) in July. Near the end of the year, La Niña's effect on the Antarctic circulation was apparent, with anomalies (low temperatures and geopotential heights, stronger westerly winds) first starting in the stratosphere in November, and then propagating downward to the surface in December. These La Niña-related anomalies were more than 1 standard deviation from the 1979–2006 mean, and the fact that they began earlier in the stratosphere suggests the stratosphere may play a role in coupling the ENSO and the SAM, as seen in earlier austral summers (e.g., L'Heureux and Thompson 2006; Fogt and Bromwich 2006).

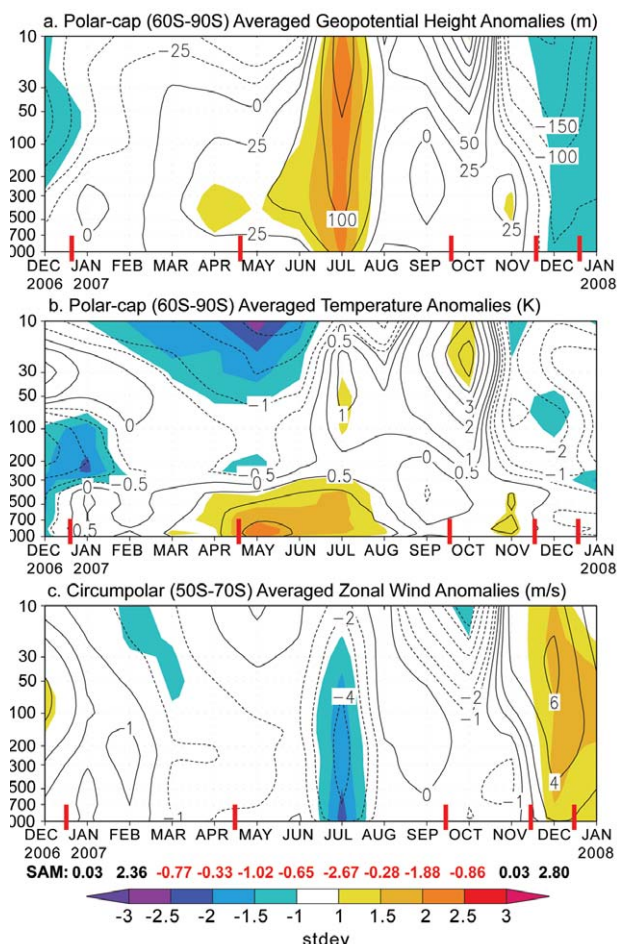


FIG. 5.21. Zonally averaged climate parameter anomalies for the southern polar region in 2007 relative to the 1979–2006 period: (a) Polar cap averaged geopotential height anomalies (m); (b) averaged temperature anomalies (K); (c) averaged wind anomalies (m s^{-1}). Absolute anomaly values are contoured, and the panels are tinted according to the standard deviation of the anomaly (color bar at bottom for scale). Red vertical bars indicate the four separate periods shown as spatial climate anomalies for 2007 in Fig. 5.22 (section 5b2). Primary contour interval is 50 m in (a), 1 K in (b), and 2 m s^{-1} in (c), with selected additional contours at $\pm 25 \text{ m}$, $\pm 0.5 \text{ K}$, and $\pm 1 \text{ m s}^{-1}$ in (a), (b), and (c), respectively. Values for the SAM index are shown along the bottom in black and red (SAM values are from www.nerc-bas.ac.uk/icd/gjma/sam.html).

Although many uncertainties exist regarding the mechanisms of climate pattern changes in each polar region, a few factors appear to play dominant roles in the circulation response to external forcing. Important among these is the contrast in orography in the Arctic and Antarctic, leading to very different patterns of Rossby wave propagation (including the stability of tropical teleconnections). Meridional

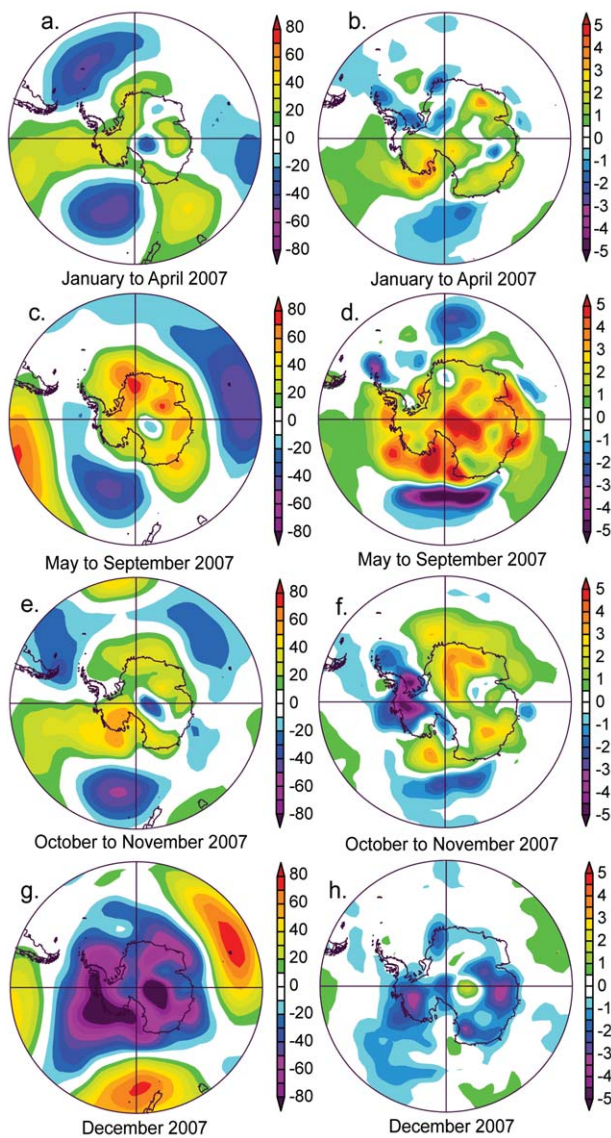


FIG. 5.22. (left) The 850-hPa geopotential height anomaly and (right) surface temperature anomaly relative to 1979–2006 climatology for four distinctive periods in 2007. Note that station data for a station near 85°S, 120°E are suspect, particularly for its geopotential height observation, in all NCEP data here.

mountain ranges and the distribution of land and oceans in the Northern Hemisphere generate strong standing wave patterns, while the Southern Ocean and nearly zonally symmetric Antarctic continent allow for generally stronger zonal flow and annular patterns. Further, stratospheric ozone depletion is playing a more crucial role in the Antarctic circulation (i.e., Thompson and Solomon 2002; Keeley et al. 2007) than in the Northern Hemisphere, and could be amplifying the changes expected from greenhouse gas forcing in some seasons (Turner et al. 2007).

3) SURFACE STATION OBSERVATIONS—S. Colwell, J. Turner, and S. Barreira

Surface observations from six representative stations across the continent (Fig. 5.23) provide a localized look at the broader atmospheric circulation patterns. The cool tendency year-round for the northern peninsula region is reflected in the negative temperature anomaly at Base Marambio (64°S, 56°W); however, on the western peninsula farther to the south, the climate was several degrees warmer than the mean through this same period (Base San Martin: 68°S, 67°W). These trends indicate a divide in mean airflow during the winter period, with generally southerly winds for the northeastern peninsula (a large deviation in direction from the norm) and northwesterly flow for the southwestern peninsula. Halley V Station (75°S, 26°W) showed a significant pressure anomaly through the winter months, which in turn is part of the pattern that drove the southerly and southeasterly flow across Marambio. Atmospheric pressure at McMurdo Station (77°S, 166°E) was unusually high in July, a trend seen across much of the continent (e.g., Halley, Mawson 67°S, 62°E, and Casey, 66°S, 110°E, as well). This was indicative of the very low SAM index, slower circumpolar westerly flow, and warm conditions seen (Fig. 5.22d).

Two extreme events of 2007 are worth noting, as an indication of how climate trends can set up strong weather anomalies. On 9 July, for the first time in 90 yr, snow was recorded in Buenos Aires, Argentina, and from that city south across Patagonia, temperatures were as much as 15°C below normal. The event was driven by a large high-pressure region just west of southern South America, flanked by two deep lows in the South Pacific and South Atlantic. The resulting winds drove warm air far to the south and into the central West Antarctic, and brought air rapidly northward from that region to the eastern flank of the Antarctic Peninsula and the southern Andes (mountain topography may have played a role in directing this flow). During the period of snowfall and cold weather in Buenos Aires, temperatures near Byrd Station AWS (near 80°S, 120°W) were as much as 16°C above normal.

Troll Station (72.02°S, 2.53°E) was the site of an extreme, and unusually long-lived, storm event during the first week of November. Surface air pressure and temperature anomalies for this period reveal that the storm was augmented by an extensive area of low pressure offshore, and high pressure to the east and south. The boundary region between these two centers sent an intense northeasterly to easterly

flow toward the station as the storm proceeded. It was likely that, again, mountain topography near the station augmented the regional flow pattern. Winds remained above 100 km h^{-1} for five consecutive days. Peak gusts reached 200 km h^{-1} , leading to significant damage at the station, including a 3,500-kg ship container that was blown several kilometers away from the base during the storm. The period during the latter part of the storm and just afterward was characterized by much warmer-than-average temperatures, as much as 16°C above the mean.

4) SURFACE MASS BALANCE—A. Monaghan and D. Bromwich

Snowfall accumulation is the mass input to the Antarctic ice sheets, and is the net result of precipitation, sublimation/vapor deposition, drifting snow processes, and melt (Bromwich 1988). Of these, precipitation is the dominant term of the Antarctic surface mass balance at regional and larger scales (Genthon 2004). To date, atmospheric models have been the most widely used means of assessing the temporal variability of the Antarctic snowfall for periods longer than a decade (e.g., Bromwich et al. 2004). The most recent modeling studies indicate there has been no trend in snowfall since about 1980 (Van de Berg et al. 2005; Monaghan et al. 2006).

Precipitation fields from the NCEP/DOE Reanalysis II (NN2) were employed to assess Antarctic snowfall for 2007. The snowfall in NN2 has been found to have an anomalously upward trend from 1979 onward compared to other model-based records and measurements from snow-stake farms and ice core records (Bromwich et al. 2004); however, the inter-annual variability of the snowfall is in very good agreement with other models (Monaghan et al. 2006). Therefore, if detrended, the NN2 record roughly approximates the “flat” trends that more accurate models predict, and the 2007 snowfall can be compared to the average for 1979–2007 to give a

proxy of whether the snowfall for the year was above or below the mean.

Figure 5.24 shows the 2007 detrended annual precipitation anomalies from the 1979–2007 mean. In general, the anomalies over the continent were negative, consistent with above average annual 850-hPa geopotential height anomalies (which indicate lower-than-normal synoptic activity) over nearly the entire continent (Fig. 5.20a). Conversely, precipitation anomalies over the Antarctic Peninsula and near the front of the Ross Ice Shelf and Marie Byrd Land ($\sim 135^\circ\text{W}$) were positive, consistent with lower-than-normal geopotential height anomalies nearby. Overall the pattern was very similar to 2006.

The 2007 detrended monthly precipitation anomalies from the 1979–2007 mean, averaged over the grounded Antarctic ice sheets, were also derived (not shown). None of the anomalies exceeded two standard deviations, but the anomalies in February, November, and the annual anomaly varied from the mean by more than one standard deviation. Continent-wide precipitation was below average during winter and spring 2007. This may have been due to below-normal synoptic activity during these months as indicated by positive 850-hPa geopotential height

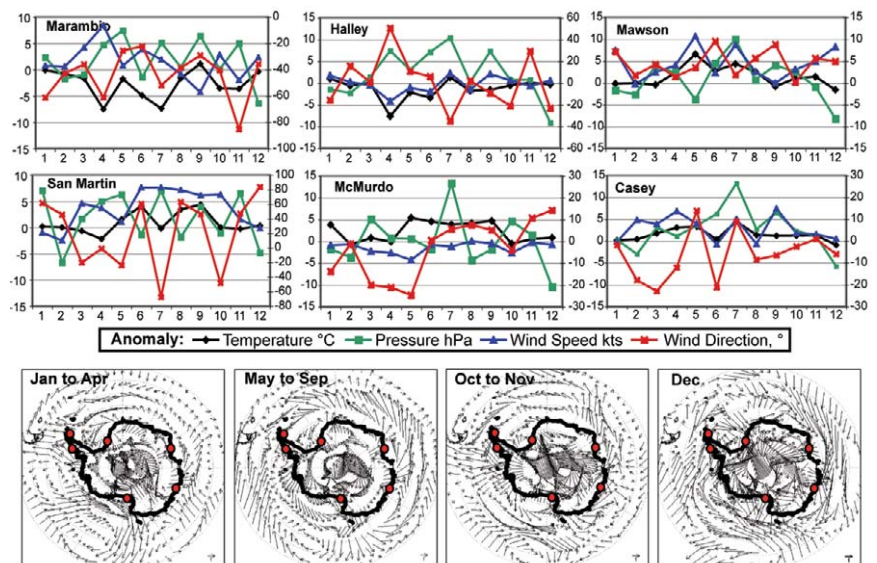


FIG. 5.23. (top) Antarctic station data and surface wind anomalies for 2007. Monthly mean anomalies for air temperature, sea level pressure, wind speed, and wind direction are shown for six representative stations. Wind direction anomaly is given in degrees clockwise (+) or anticlockwise (–) along the right-side y axis for the plots. (bottom) Mean wind direction and intensity anomaly (vector difference from mean) for the four climatological periods identified in Fig. 5.22 (section 5b2). Red dots indicate the six station locations. Reference vector is 1 km h^{-1} ($\approx 1.85 \text{ kt}$). The base period used for all plots is 1991–2000.

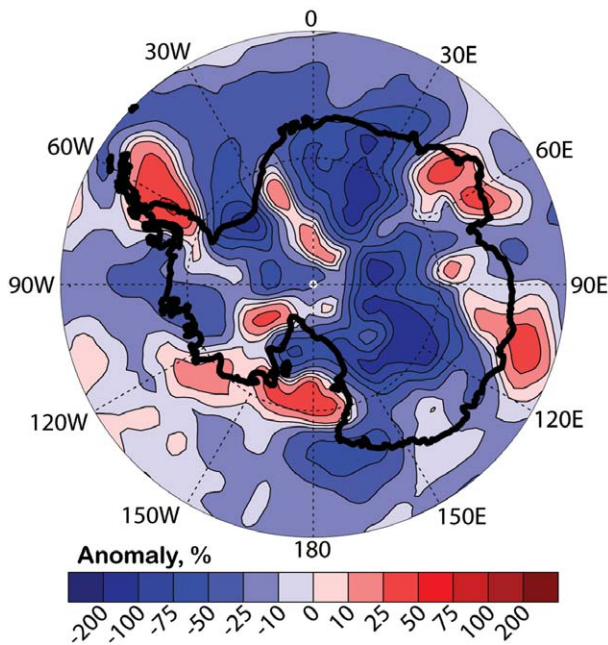


FIG. 5.24. Detrended precipitation anomalies ($\% \text{ yr}^{-1}$) from the NCEP–DOE Reanalysis II for 2007 compared with the 1979–2007 mean.

anomalies across the continent and near the coastal margins (Fig. 5.22c), which projected strongly onto the annual mean. Overall, the 2007 annual precipitation was about 7% below normal. This downward fluctuation had a positive contribution to sea level of approximately 0.35 mm.

The 2006 annual precipitation anomaly at the continental scale was similarly below normal, by 6% (Arguez et al. 2007). However, the causality of the similar annual precipitation between the two years appears to have been due to different reasons, as the 850-hPa annual and seasonal anomalies were quite different. For example, precipitation was above normal during April/May 2007, while it was below normal during the same period in 2006; weaker SAM conditions during austral autumn 2007 led to enhanced penetration of maritime air at that time.

5) SEASONAL MELT EXTENT AND DURATION—H. Liu, L. Wang, and K. Jezek

Using a wavelet transform–based edge detection method (Liu et al. 2005), the extent, onset date, end date, and duration of snow melt on the Antarctic ice sheet during the 2006–07 austral summer were derived. The 19-GHz horizontal polarization channel of satellite passive microwave data (SSM/I, a sensor flown on several U.S. defense meteorological satellites) is utilized for the melt information extraction. Melt onset date, duration, and extent are shown in Fig. 5.25. The total melt extent during the austral year 2006–07 was 900,625 km^2 , covering only 6.6% of the continent. This was determined by summing all pixels with at least one day of surface melting. The melt index during 2006–07 (sum of total melt extent for each day in the melt season; Liu et al. 2006) was 28,011,250 day km^2 . As shown in Fig. 5.25c, there has been a decreasing trend in melt extent the past five years, and for the overall record (1978–2007). The austral year 2006–07 melt extent, and intensity (melt index) rank the second lowest since 1978.

The surface melt during 2006–07 mainly occurred on the Antarctic Peninsula, Abbot Ice Shelf, West Ice Shelf, Shackleton Ice Shelf, and Amery Ice Shelf. A brief but extensive surface melting was detected over the Ronne–Filchner Ice Shelf during January 2007. Amery Ice Shelf, Queen Maud Land, Wilkes Land, and Ross Ice Shelf have an extremely low melt

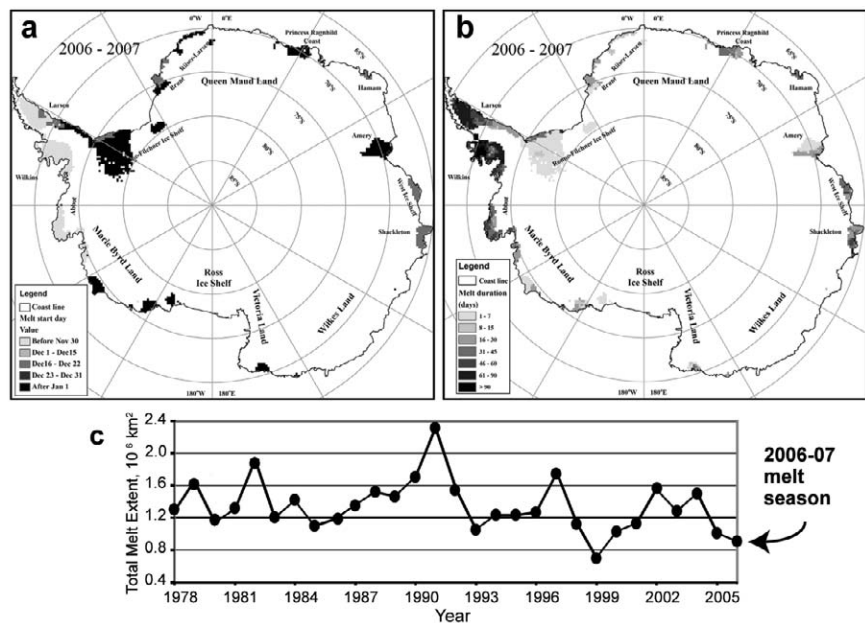


FIG. 5.25. (a) Melt onset date and (b) melt season duration in days, for the 2006–07 melt season. The sum of the regions indicated in both plots indicates total melt extent for the year as shown in the (c) graph of total melt extent.

extent and melt intensity. Surface melt primarily took place in December, January, and February, and the extent peaked on 21 January 2007.

6) SEA ICE EXTENT AND CONCENTRATION—R. A. Massom, P. Reid, S. Barreira, and S. Stammerjohn

Antarctic sea ice in 2007 was characterized by considerable temporal and spatial variability, with ice extent anomalies ranging from a record low in May of -12% or $-1.2 \times 10^6 \text{ km}^2$ (equal to 1980) to a record high in December of $+14\%$ or $+1.7 \times 10^6 \text{ km}^2$ for the satellite time series (1978–present; Fig. 5.26). The analysis is based on monthly mean SSM/I-derived sea ice concentration data produced by the NSIDC Sea Ice Index project (Fetterer et al. 2002, updated monthly).

With the exception of May, sea ice extent overall was generally close to or only slightly lower than the long-term mean for January through August. There was, however, considerable regional variability, largely in response to the strong circulation and temperature patterns described earlier. This resulted in sea ice extent and concentration anomalies that were both greater and zonally asymmetric (Fig. 5.26).

A strong feature of the 2007 austral minimum ice extent period (January–March) was the persistence of zones of high concentration ice in the east Weddell Sea, the Ross Sea, around the BI, and along the Indian Ocean coastal sector (Fig. 5.26a). Conversely, significantly less

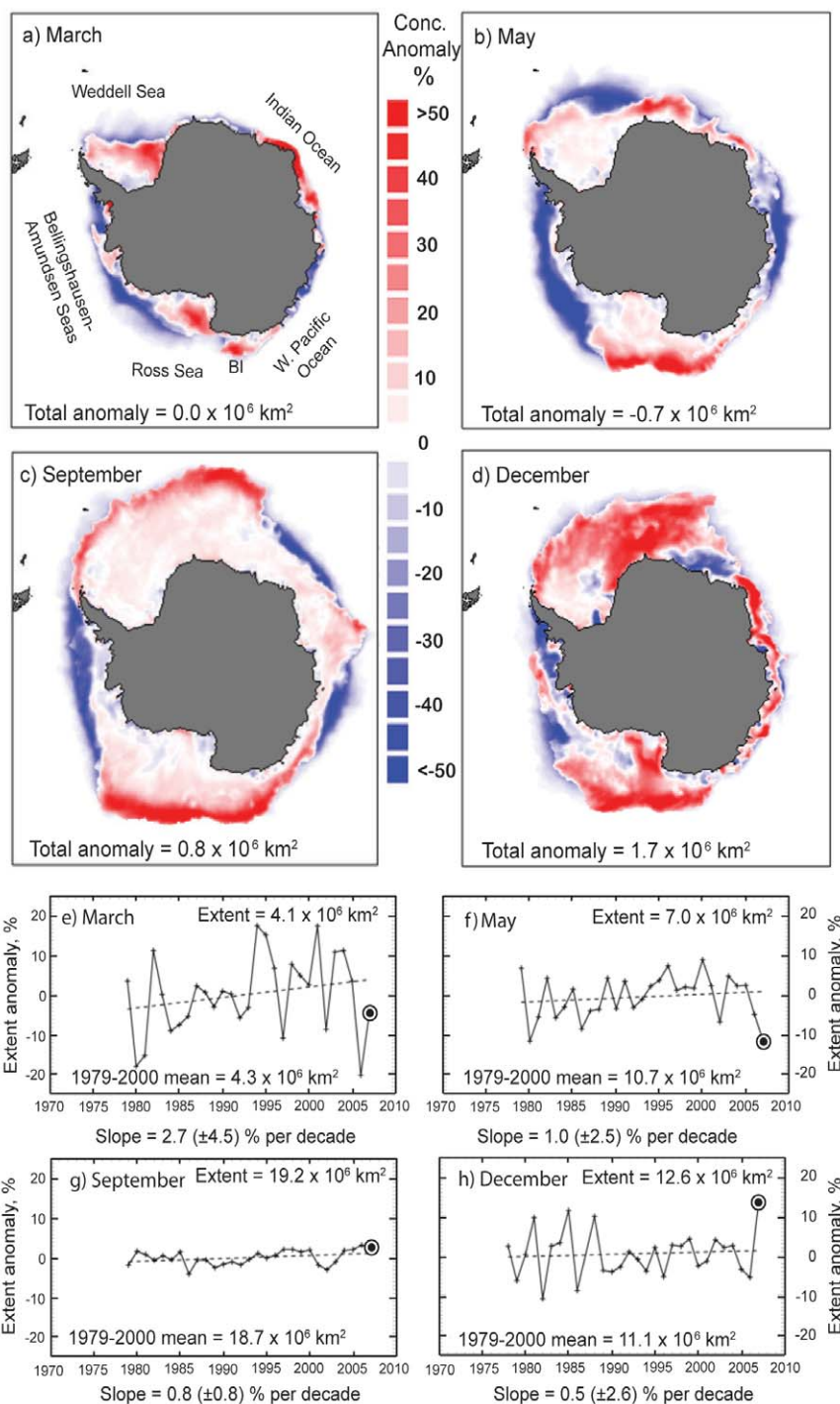


FIG. 5.26. Antarctic sea ice concentration anomalies in 2007 relative to the 1979–2000 mean for the month for (a) Mar, (b) May, (c) Sep, and (d) Dec, and (e)–(h) trends in sea ice extent for the same months. “BI” in (a) indicates the Balleny Islands area. Sea ice concentration is the area covered by ice per unit area. Concentration is derived for 25-km grid cells; the color mapped monthly concentration anomalies are the difference between the 2007 value and the 1979–2000 mean value for those grid cells. The total concentration anomaly is the sum of anomalies over all grid cells. Ice extent is the total area covered by ice at any concentration. From the Sea Ice Index (http://nsidc.org/data/seai_index/).

ice occurred in the Amundsen Sea and west Pacific Ocean sectors at this time compared to the mean.

The distinctive zonal asymmetry in ice extent and concentration anomalies was particularly well developed in May (Fig. 5.26b). The record negative extent anomaly at this time, which represents a strong departure from the upward trend for ice extent in this month (Fig. 5.26f), resulted from lower-than-average autumnal advance over broad zones across the Weddell Sea, the sector 70°–110°E, and the Bellingshausen–Amundsen Seas. The latter was associated with a persistent, deep low pressure circulation centered on approximately 70°S, 135°W—the “Amundsen Sea Low.” This created a persistent and dominant west-northwesterly airflow that led to compaction of the sea ice against the West Antarctic Peninsula and Amundsen Sea coasts, preventing normal autumnal ice edge advance (see Massom et al. 2008). Conversely, cold air outflow to the west from continental Antarctica resulted in an ice edge advance and a positive ice concentration anomaly across the Ross Sea sector.

The remainder of the year (September–December) was characterized by similar regional patterns in negative and positive ice extent, area, and concentration anomalies (Figs. 5.26c,d), but with overall extent anomalies becoming positive (Figs. 5.26g,h). At $19.2 \times 10^6 \text{ km}^2$, ice extent in September was 3% above the 1979–2000 September mean; this was the second highest extent on record (just behind 2006 at $19.35 \times 10^6 \text{ km}^2$), but the highest in terms of areal coverage, that is, the product of ice extent and concentration (at $15.2 \times 10^6 \text{ km}^2$ versus $15.1 \times 10^6 \text{ km}^2$ for September 2006). As was the case in May, a major determinant of the wide zone of negative extent and concentration anomalies across the Bellingshausen–Amundsen Seas sector was wind-driven compaction associated with a deep Amundsen Sea low air pressure anomaly, this time coupled with a blocking high-pressure anomaly in the South Atlantic.

Spatially, the August through October sea ice extent showed, in most areas, a continuation of the long-term trend in Southern Hemisphere sea ice extent for those months. For example, sea ice extent to the north of the Ross Sea continued to expand during these months, while farther to the east there was a contraction of ice extent. Both anomalies were primarily a result of deepening low pressure in the Amundsen Sea. Interestingly, in the far southwest of the Indian Ocean, sea ice extent was anomalously low, in contrast to the long-term trend in that area. This was primarily due to the central low pressure system being farther to the west than normal in that region. Both January and December 2007 had a continuation of the trend in

lowering sea ice concentration around Davis Station (68° 35'S, 77° 58'E) and an increase in sea ice concentration around Mawson (67° 36'S, 62° 52'E).

As noted above, the December 2007 value of +14% ($+1.7 \times 10^6 \text{ km}^2$) is the highest on record. Notable also is the SAM index value for December, which was +2.80, among the highest ever, based on observational records dating back to 1957 (www.nerc-bas.ac.uk/icd/gjma/sam.html; see also Marshall 2003). The 2007 La Niña also reached its maximum late in the year, with an SOI value¹ of 14.4 in December and the Niño-3 region reaching a minimum sea surface temperature in November. The persistence of unusually compact sea ice into the summer melt period of 2007–08 in the Weddell Sea, East Antarctic coastal, and Ross Sea sectors led to reported difficulties in ship navigation during the critical shipping (base resupply) season.

7) OZONE DEPLETION—P. A. Newman

The Antarctic ozone hole was less deep in 2007 than the severely depleted 2006 ozone hole, and was near average in comparison to the last 15 yr. The areal extent of the hole was slightly smaller than average. South Pole ozonesondes showed higher than average ozone in comparison to the last 20 yr, and the OMI measurement of the Antarctic minimum ozone value was also slightly higher than average. This slightly improved Antarctic ozone situation resulted from warmer-than-average stratospheric temperatures during the ozone loss period in September–October (Fig. 5.21b).

The ozone hole is primarily caused by human-produced compounds that release chlorine and bromine gases in the stratosphere. Observations by the *Aura* satellite's MLS showed extremely high levels of ClO chemicals in the lower stratosphere (465 K, ~20 km) during August and September. These high levels of ClO covered almost the entire Antarctic region but had been largely converted to other nonozone destroying forms by early October. Coincident with the high ClO were extremely low values of ozone.

A fundamental process behind the formation of the ozone hole is the conversion of chlorine molecules from the nonreactive forms (HCl and ClONO₂) into reactive forms on the surfaces of PSCs. This reactive chlorine leads to rapid ozone destruction. The CALIPSO satellite provides an extremely high-resolution estimate of PSC structure over Antarctica

¹ The December SOI value of 14.4 is based on nonstandardized data.

using lidar technology. Using this instrument, it is estimated that the volume of PSCs was smaller in 2007 than 2006 by about two-thirds. In addition, the presence of PSCs over Antarctica ended at a slightly earlier date at altitudes near 20 km. The smaller volume of PSCs resulted in less conversion to reactive chlorine, and hence a smaller ozone hole in 2007 than 2006.

Over the last 15 yr, the ozone hole has reached an average yearly maximum size of about 23–24 million km². On 13 September 2007 the Antarctic ozone hole reached an areal extent of 25.1 million km². For the period 21–30 September, the area of the ozone hole was almost in the average range at 22.8 million km². The minimum values of ozone inside the ozone hole were also higher than the last few years (the record low value occurred in 2006, at 85 Dobson units on 8 October). In 2007 the lowest value observed by OMI was 106 Dobson units on 30 September. The spatial extent of the hole on this day is shown in Fig. 5.27.²

Balloon-borne ozonesonde observations from NOAA/ESRL at the South Pole showed a low ozone value of 125 Dobson Units on 8 October 2007. The layer between 14 and 21 km had a typical 95% loss of ozone. This contrasts with a value of 93 Dobson units on 9 October 2006 and essentially complete destruction in the 14–21-km layer. These balloon measurements also showed that temperatures in the critical layer of 20–24 km were below average in early September, but warmed to above average values in mid-September.

The severity of the ozone hole varies from year to year with the temperature of the Antarctic stratosphere. Colder than average temperatures result in larger and deeper ozone holes, while warmer temperatures lead to smaller size and less ozone destruction. NOAA satellite temperatures and balloon temperatures during the late-September 2007 period indicated that the lower-stratospheric temperatures at the rim of Antarctica (65°–75°S, 20 km) were almost equal to the long-term temperature average of 198 K.

As a result of regulations, the concentrations of ozone depleting substances in the lower atmosphere (troposphere) peaked in about 1995 and are now de-

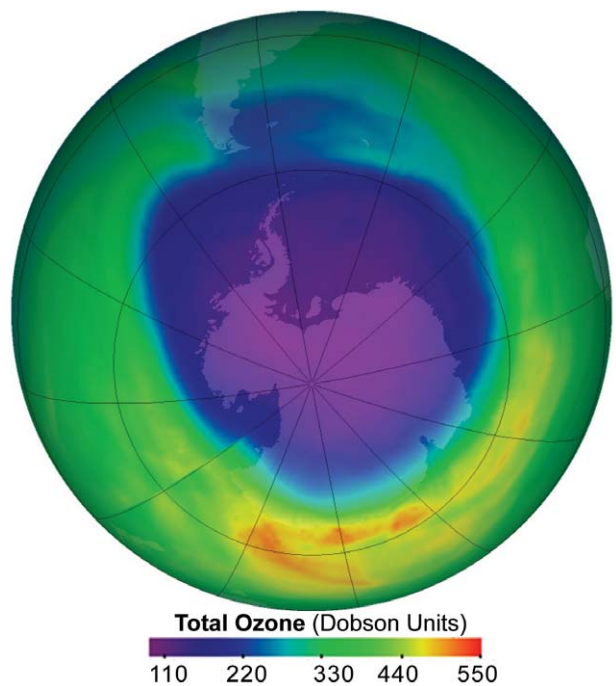


FIG. 5.27. Total ozone (in DU) measured on 30 Sep 2007. Purple blue coloring indicates the low values of the Antarctic ozone hole. The minimum value observed on this day was 106 DU. The image is based on total ozone observations from the OMI aboard the NASA Aura satellite. From Ozone Hole Watch (<http://ozonewatch.gsfc.nasa.gov/>).

creasing in both the troposphere and stratosphere. It is estimated that these gases reached peak levels in the Antarctic stratosphere in 2001 and are now slowly decreasing. However, these ozone depleting substances typically have very long lifetimes in the atmosphere (>40 yr). The chlorine and bromine gases are now slowly decreasing from peak levels by about 0.7% yr⁻¹ (down only 3.1% from the 2001 peak). As a result of this slow decline of ozone depleting substances, the ozone hole is estimated to be very slowly decreasing in area by about 0.2% yr⁻¹. This slow decrease is masked by the large year-to-year variations caused by the Antarctic stratospheric weather fluctuations (Newman et al. 2006).

The Antarctic stratosphere is warmed by the return of sunlight at the end of the polar winter and by large-scale weather systems (planetary-scale waves) that form in the troposphere and move upward into the stratosphere. During the 2007 Antarctic winter and spring, these planetary-scale wave systems were stronger than normal (10%–15% above average for the August–September period). Because the wave levels were above average in 2007, the Antarctic stratospheric temperature was also slightly above average.

² The analysis was based upon data from the NASA *Aura* satellites, in particular, the KNMI OMI and the JPL MLS. PSC information was obtained from the NASA LaRC CALIPSO instrument. NOAA/NCEP provided analyses of satellite and balloon stratospheric temperature observations. NOAA/ESRL regularly launches ozone- and temperature-measuring balloon instruments from the South Pole.